Published in final edited form as:
J Nucl Med. 2013 July ; 54(7): 1120–1126. doi:10.2967/jnumed.112.113217.

^{18}F-AFETP, ^{18}F-FET, and ^{18}F-FDG Imaging of Mouse DBT Gliomas

Kiran Kumar Solingapuram Sai[1,*], **Chaofeng Huang**[1,*], **Liya Yuan**[2], **Dong Zhou**[1], **David Piwnica-Worms**[1,3], **Joel R. Garbow**[1], **John A. Engelbach**[1], **Robert H. Mach**[1], **Keith M. Rich**[2], and **Jonathan McConathy**[1]

[1]Department of Radiology, Washington University School of Medicine, St. Louis, Missouri

[2]Department of Neurosurgery, Washington University School of Medicine, St. Louis, Missouri

[3]BRIGHT Institute, Washington University School of Medicine, St. Louis, Missouri

Abstract

The goal of this study was to evaluate the ^{18}F-labeled nonnatural amino acid (*S*)-2-amino-3-[1-(2-^{18}F-fluoroethyl)-1*H*-[1,2,3]triazol-4-yl]propanoic acid (^{18}F-AFETP) as a PET imaging agent for brain tumors and to compare its effectiveness with the more-established tracers *O*-(2-^{18}F-fluoroethyl)-L-tyrosine (^{18}F-FET) and ^{18}F-FDG in a murine model of glioblastoma. The tracer ^{18}F-AFETP is a structural analog of histidine and is a lead compound for imaging cationic amino acid transport, a relatively unexplored target for oncologic imaging.

Methods—^{18}F-AFETP was prepared using the click reaction. BALB/c mice with intracranially implanted delayed brain tumor (DBT) gliomas (n = 4) underwent biodistribution and dynamic small-animal PET imaging for 60 min after intravenous injection of ^{18}F-AFETP. Tumor and brain uptake of ^{18}F-AFETP were compared with those of ^{18}F-FDG and ^{18}F-FET through small-animal PET analyses.

Results—^{18}F-AFETP demonstrated focally increased uptake in tumors with good visualization. Peak tumor uptake occurred within 10 min of injection, with stable or gradual decrease over time. All 3 tracers demonstrated relatively high uptake in the DBTs throughout the study. At late time points (47.5–57.5 min after injection), the average standardized uptake value with ^{18}F-FDG (1.9 ± 0.1) was significantly greater than with ^{18}F-FET (1.1 ± 0.1) and ^{18}F-AFETP (0.7 ± 0.2). The uptake also differed substantially in normal brain, with significant differences in the standardized uptake values at late times among ^{18}F-FDG (1.5 ± 0.2), ^{18}F-FET (0.5 ± 0.05), and ^{18}F-AFETP (0.1 ± 0.04). The resulting average tumor-to-brain ratio at the late time points was significantly higher for ^{18}F-AFETP (7.5 ± 0.1) than for ^{18}F-FDG (1.3 ± 0.1) and ^{18}F-FET (2.0 ± 0.3).

Conclusion—^{18}F-AFETP is a promising brain tumor imaging agent, providing rapid and persistent tumor visualization, with good tumor–to–normal-brain ratios in the DBT glioma model. High tumor-to-brain, tumor-to-muscle, and tumor-to-blood ratios were observed at 30 and 60 min after injection, with higher tumor-to-brain ratios than obtained with ^{18}F-FET or ^{18}F-FDG. These results support further development and evaluation of ^{18}F-AFETP and its derivatives for tumor imaging.

For correspondence contact: Jonathan McConathy, 510 S. Kingshighway Blvd., Campus Box 8223, St. Louis, MO 63110. mcconathyj@mir.wustl.edu.
*Contributed equally to this work.

DISCLOSURE
The Siteman Cancer Center is supported in part by NCI Cancer Center Support Grant #P30 CA91842. This research was funded by the National Cancer Institute (K08CA154790; P50CA94056) and the Mallinckrodt Institute of Radiology. No other potential conflict of interest relevant to this article was reported.

Keywords

click reaction; amino acid; glioma; ^{18}F

Radiolabeled amino acids (AAs) have long been recognized as useful tumor imaging agents, and several tracers, including L-^{11}C-methionine and *O*-(2-^{18}F-fluoroethyl)-L-tyrosine (^{18}F-FET), have been used clinically, particularly for brain tumors. These tracers target the increased rates of amino acid transport present in many types of tumor cells. In the brain, these tracers provide better tumor visualization than the most widely used PET tracer for oncology, ^{18}F- FDG, and contrast-enhanced MR imaging alone (1–5). There are also data suggesting that ^{18}F-FET PET can differentiate low-grade from high-grade gliomas and can more accurately evaluate tumor response to therapy earlier in the course of treatment than MR imaging (3,6–10). There has been a growing appreciation that radiolabeled AAs targeting different AA transport systems have distinct imaging properties and may provide unique biologic information relevant to prognosis and therapy (11–14).

The bulk of work performed with radiolabeled AAs has focused on substrates for system L AA transport, which preferentially transports AAs with bulky neutral side chains like L-leucine, L-tyrosine, and L-phenylalanine through an energy-independent exchange mechanism. To date, more than 20 AA transporter systems have been identified with varying specificities for substrates, sodium and pH dependences, and tissue-expression patterns. Major transport systems recognized as relevant to tumor imaging include system L, system A, and system ASC (14–16).

Recently, there has been growing interest in other AA transport systems, including xCT, glutamine, and cationic AA transporters (17–20). Our group recently reported a novel ^{18}F-labeled AA synthesized through the click reaction, (*S*)-2-amino-3-[1-(2-^{18}F-fluoroethyl)-1*H*-[1,2,3]triazol-4-yl]propanoic acid (^{18}F-AFETP). This tracer is a structural analog of histidine and showed promising tumor imaging properties in the rat 9 L gliosarcoma model, which has been used for the preclinical evaluation of several radio-labeled AAs (21–24). The in vitro uptake of this compound was mediated, in part, by cationic AA transport, and ^{18}F-AFETP represents a lead compound for a new class of radiolabeled AA for tumor imaging. The transport was stereospecific, and the (*R*)-enantiomer of AFETP demonstrated lower tumor uptake and tumor–to–normal-tissue ratios (22).

Although relatively unexplored, cationic AA transport is an attractive target for oncologic imaging. Specific cationic AA transporters are upregulated in human cancers including cervical and colorectal (25,26). The cationic AA transporter CAT-1 is active at the blood–brain barrier (BBB), possibly allowing visualization of the nonenhancing regions of gliomas (27). Cationic AA transporters recognize L-lysine, L-arginine, and L-histidine as substrates, and both L-lysine and L-histidine are essential AAs that cannot be synthesized by human cells. L-arginine is conditionally essential in rapidly dividing cells and in cells that lack the enzyme arginosuccinate synthase (ASS), which is absent in a range of human cancers and is a target for therapy using arginine deiminase (28,29). Additionally, L-arginine plays important roles in polyamine synthesis and nitric oxide metabolism, which are relevant to tumor cell proliferation and angiogenesis, respectively. The roles of cationic AA transport and metabolism for predicting prognosis, selecting therapies, and monitoring response to therapy are not currently defined in large part because of the lack of well-characterized molecular imaging agents for purpose.

To further assess the utility of ^{18}F-AFETP for tumor imaging, this tracer was evaluated in the mouse delayed brain tumor (DBT) model, a syngeneic murine model of glioblastoma (30). The tumor imaging properties of ^{18}F-AFETP were evaluated in mice with intracranial DBTs through biodistribution and small-animal PET/CT studies. Additionally, the tumor and brain uptake of ^{18}F-AFETP was compared with those of ^{18}F-FDG and ^{18}F-FET (Fig. 1) through small-animal PET studies because these tracers are clinically relevant and used for brain tumor imaging in patients.

MATERIALS AND METHODS

Radiosynthesis

^{18}F-FDG was produced by the Washington University Cyclotron Facility. ^{18}F-AFETP and ^{18}F-FET were radiosynthesized using literature methods with minor modifications (22,31). ^{18}F-fluoride was produced from ^{18}O-H_2O using an RDS 111 cyclotron (CTI) through the ^{18}O(p,n)^{18}F reaction.

^{18}F-AFETP (**3**) was prepared in a 2-step reaction starting from 2-^{18}F-fluoroethyl azide and *tert*-butyl ester of *N*-Boc-(*S*)-propargyl glycine (**1**) based on the previously published procedure with minor modifications, as depicted in Figure 2 (22). The crude ^{18}F-labeled protected intermediate **2** was injected directly onto the Agilent Zorbax C18 semipreparative high-performance liquid chromatography (HPLC) column (250 × 10 mm, 10 μm) without isolation through a reversed-phase cartridge (Waters, Inc.), as in the original report. A larger volume of 1.0 M aqueous hydrochloric acid (1.0 mL) was used for the microwave-assisted deprotection of the intermediate to eliminate the intermittent presence of a minor radiochemical impurity in the final product. For cell uptake assays, the acidic solution was evaporated to dryness by heating to 105°C with nitrogen gas flow, and ^{18}F-AFETP was dissolved in sterile water to avoid the presence of sodium ions. For the rodent studies, the acidic solution was neutralized through the addition of 1.0 M aqueous sodium bicarbonate (1.0 mL), passed through a 0.22-μm nylon filter, and then diluted in 0.9% sodium chloride for injection. The radiochemical purity and specific activity of ^{18}F-AFETP were confirmed using radiometric thin-layer chromatography and HPLC analyses including the coinjection of non-radioactive reference compound. ^{18}F-FET was performed with the commercially available Eckert and Ziegler Modular Lab using the method described by Zuhayra et al. with a 1-bromo-2-^{18}F-fluoroethane for *O*-alkylation of the L-tyrosine (32).

Cell Uptake Assays

Cell uptake assays were performed using the cluster-tray method as reported in the literature (22,33). Mouse DBT glioma cells were cultured at 1×10^5 per 24 well (Corning) for 48 h in a 5% CO_2 atmosphere in 10% fetal bovine serum–Dulbecco modified Eagle medium. Two buffer conditions, with and without sodium, were used for the assays. The phosphate-buffered saline solution contained 105 mM sodium chloride, 3.8 mM potassium chloride, 1.2 mM potassium bicarbonate, 25 mM sodium phosphate dibasic, 0.5 mM calcium chloride dihydrate, 1.2 mM magnesium sulfate, and 5.6 mM D-glucose. The sodium-free, phosphate-buffered choline solution was identical to the phosphate-buffered saline solution except that choline chloride and choline phosphate dibasic were substituted for sodium chloride and sodium phosphate dibasic, respectively.

The following inhibitors were used for the cell uptake assays: *N*-methyl-α-aminoisobutyric acid (MeAIB, 10 mM), a mixture of L-alanine/L-serine/L-cysteine (ASC, 3.3 mM of each AA), (*R,S*)-(endo,exo)-2-aminobicyclo(2,2,1)-heptane-2-carboxylic acid (BCH, 10 mM), L-arginine (10 mM), L-lysine (10 mM), L-histidine (10 mM), and a mixture of L-arginine/L-lysine/L-histidine (RKH, 3.3 mM of each AA). The control conditions contained 10 mM

sucrose to maintain consistent osmolality. All assays were performed in quadruplicate at pH 7.40, as described previously (22,33). The uptake data were expressed as percentage of uptake relative to control, normalized to total protein content in each well. The data were analyzed with 1-way ANOVA with Tukey multiple pairwise comparisons using GraphPad Prism software (GraphPad Software), with *P* values of 0.05 or less considered statistically significant.

DBT Model

All animal experiments were conducted according to protocols approved by the Animal Studies Committee at the Washington University School of Medicine.

The DBT model was chosen because it exhibits many features of human glioblastomas. These tumor cells are positive for glial fibrillary acidic protein and are highly motile. Orthotopic DBTs in mouse brain have been previously characterized in studies comparing MR imaging, bioluminescence, and histologic measurements of tumor volume (30). The DBT cells (1×10^4 cells suspended in 8 μL) were implanted in the right mid cerebrum of male BALB/c mice (20–25 g) at 2 mm posterior to the bregma, as described previously (34). The DBT cell line constitutively expresses the enzyme luciferase. The presence of viable DBTs was confirmed through bioluminescence imaging, and animals were sorted on the basis of tumor size and location into matched cohorts before imaging studies, as described previously (30,35).

Biodistribution Studies with ^{18}F-AFETP

Biodistribution studies were performed using male BALB/c mice with intracranial DBTs at 13 d after implantation. Mice were anesthetized with 1% isoflurane–oxygen, and approximately 1.1 MBq of ^{18}F-AFETP was administered via tail vein injection. The animals were euthanized in groups of 3 or 4 at 5, 30, and 60 min after injection. The tumors, organs, and tissues of interest were dissected and weighed, and the amounts of radioactivity were measured using an automated Beckman γ-8000 well counter. Additionally, radioactive standards from the dosages were counted. The concentrations of radioactivity in the tumors and the normal organs and tissues normalized as percentage injected dose per gram (%ID/g) of radioactivity in the tumors and the normal organs and tissues as well as ratios of tumor to normal organ and tumor to normal tissue were calculated. The data for blood, brain, muscle, and tumor were analyzed for each time point with 1-way ANOVA with Tukey multiple pairwise comparisons using GraphPad Prism software.

MR Imaging

MR imaging experiments were performed on 4 mice with intracranial DBTs at day 12 after implantation. Data were collected on a dedicated small-animal MR scanner built around an Oxford Instruments 4.7-T magnet, using an Agilent/Varian DirectDrive console, high-performance Agilent/Magnex gradients, and International Electric Co. gradient power supplies. Mice were anesthetized with isoflurane–O_2 (2%–3% [v/v]) and maintained on isoflurane–O_2 (1% [v/v]) throughout the experiments. Animal body temperature was maintained at 37°C with warm, circulating water. Mice were injected intraperitoneally with 500 μL of MultiHance (Bracco Diagnostics, Inc.) contrast agent, diluted 1:10 in sterile saline, 15 min before being placed in the magnet. T2-weighted, spin-echo MR images were collected with the following parameters: repetition time, 2 s; echo time, 0.03 s; field of view, 1.5×1.5 cm^2; slice thickness, 0.5 mm; number of averages, 4; and data matrix, 128×128.

Small-Animal PET/CT Imaging

Male BALB/c mice ($n = 4$) with intracranial DBTs were anesthetized with 1% isoflurane–O_2. The mice then underwent dynamic small-animal PET imaging from 0 to 60 min after intravenous tail injection of 7.4–11.1 MBq of ^{18}F-AFETP on day 14 and 11.1 MBq of ^{18}F-FDG on day 15 after tumor implantation, using Inveon and microPET Focus 220 systems (Siemens Medical Solutions Inc.). The animals were fasted overnight before the ^{18}F-FDG studies and allowed to feed ad libitum before the ^{18}F-AFETP and ^{18}F-FET studies. The animals were maintained at 37°C during the study using a warming lamp. CT images were also acquired with the Inveon system. A separate cohort of male BALB/c mice ($n = 4$) with intracranial DBTs underwent the same imaging protocol after the administration of 7.4–11.1 MBq of ^{18}F-FET. At the conclusion of the imaging studies, the animals were euthanized, and their brains were fixed for 24–48 h in 4% paraformaldehyde for histologic analysis with hematoxylin and eosin staining to verify the presence and location of tumor.

The small-animal PET data were analyzed by manually drawing 3-dimensional regions of interest (ROIs) over the tumor identified on the PET studies, with correlation to MR imaging and histology to confirm the tumor location. ROIs for normal brain were drawn over the cerebral hemisphere contralateral to the tumor. The ROIs for the tumors ranged from 13 to 30 mm^3, and comparable ROIs were drawn over the contralateral normal brain. The uptake data were expressed as average standardized uptake values (SUVs) for each ROI. The average of the SUVs in brain and tumor, as well as the average of the tumor-to-brain ratios at 50–60 min after injection for ^{18}F-AFETP, ^{18}F-FDG, and ^{18}F-FET, were compared with 1-way ANOVA with Tukey multiple pairwise comparisons using GraphPad Prism software.

RESULTS

Radiochemistry

^{18}F-AFETP was produced in 58% ± 4% ($n = 6$) decay-corrected yield in a total synthesis and formulation time of approximately 2.5 h, using the modified procedure. As in the original report, the enantiomeric excess, as assessed by analytic chiral HPLC, was greater than 98%, with the undesired (*R*)-enantiomer below the limits of detection. The overall radiochemical purity was greater than 99%, and the specific activity of the ^{18}F-AFETP was approximately 44 GBq/μmol ($n = 6$), decay-corrected to the end of bombardment. For ^{18}F-FET, the final radiotracer was purified using HLB reversed-phase cartridges (Waters, Inc.) in an average radiochemical yield of 27%, with a greater than 98% radiochemical purity and greater than 37 GBq/μmol specific activity ($n = 4$).

Cell Uptake Assays

The results of the in vitro cell uptake assays are displayed in Figure 3. In the presence of 10 mM L-histidine or 10 mM L-lysine, 87% and 77% of ^{18}F-AFETP uptake by DBT cells, respectively, was blocked. In the assay buffer containing choline ions, ^{18}F-(*S*)-AFETP demonstrated an inhibition of 62%. In the ASC condition, approximately 50%–58% of uptake was inhibited. The variability observed between the ASC conditions in different assays (50% ± 8% and 42% ± 4%) is within experimental error for this type of assay. A minor, but statistically significant, inhibition of uptake was observed with the system A inhibitor MeAIB and the system L inhibitor BCH.

Biodistribution Studies with ^{18}F-AFETP

The results of biodistribution studies with ^{18}F-AFETP in male BALB/c mice are shown in Table 1. The tumor uptake after injection was rapid, with 4.4 ± 1.1 %ID/g at 5 min. There was persistent retention of activity in the tumor at the 30-min time point (4.9 ± 1.2 %ID/g), which decreased slightly to 2.5 ± 1.0 %ID/g at 60 min. The %ID/g of ^{18}F-AFETP was

significantly higher than normal brain and muscle at all time points and higher than blood at 30 and 60 min after injection (P <0.001). The resulting tumor-to-brain ratios at the 5-, 30-, and 60-min time points were 17:1, 14:1, and 11:1, respectively. The tumor–to–normal-tissue ratios at 30 and 60 min after injection were greater than 2:1 for the blood, bone fat, liver, muscle, and large intestine.

Small-Animal PET Studies in Mice with DBTs

Representative small-animal PET and MR images obtained with ^{18}F-AFETP, ^{18}F-FDG, and ^{18}F-FET are presented in Figure 4, and representative time–activity curves are shown in Figure 5 as average SUVs and tumor-to-brain ratios over time. The PET studies revealed a significant difference in uptake and kinetics in DBT and normal brain for all 3 tracers. Relatively high uptake occurred in the DBTs at both early (7.5–12.5 min) and late time points (47.5–57.5 min), with ^{18}F-FDG significantly greater than ^{18}F-FET greater than ^{18}F-AFETP as shown in Figure 6. These ^{18}F-labeled tracers differed substantially in their amount of uptake in normal brain, with ^{18}F-FDG significantly greater than ^{18}F-FET greater than ^{18}F-AFETP. The uptake of ^{18}F-FDG in brain tumor was only slightly above that in normal brain at the conclusion of the 60-min study. The average tumor-to-brain ratios for ^{18}F-FET, ^{18}F-AFETP, and ^{18}F-FDG at the early time points were 2.9 ± 0.2, 6.2 ± 1, and 0.9 ± 0.1, respectively, and at the late time points were 2.0 ± 0.3, 7.5 ± 1, and 1.3 ± 0.1, respectively, as depicted in Figure 7. The tumor-to-brain ratio achieved with ^{18}F-AFETP was significantly higher than with ^{18}F-FDG and ^{18}F-FET (P < 0.001 for both).

DISCUSSION

Radiochemical synthesis of ^{18}F-AFETP was achieved in high radiochemical purity and specific activity. Elimination of the solid-phase extraction step before HPLC during the radiolabeling process reduced the complexity of the synthesis. The larger volumes of 1 M aqueous HCl used for acidic deprotection and the use of evaporation, rather than ion-retardation chromatography, to obtain the final product in a sodium-free form increased the radiochemical purity of ^{18}F-AFETP, which was greater than 99%.

The cell uptake assays were performed with a short, 30-s uptake time to evaluate the initial influx of ^{18}F-AFETP and minimize the potential for efflux, which can be mediated by many AA transporters, including system L, system ASC, and the cationic AA transport families CAT and y^+L. From the in vitro cell uptake assay results (Fig. 3), the cationic AA transport substrates L-lysine and L-histidine, as well as a combination of L-arginine, L-lysine, and L-histidine, were the most effective inhibitors of ^{18}F-AFETP uptake. Together, these findings suggest that a significant proportion of the in vitro uptake of ^{18}F-AFETP is mediated by cationic AA transporters, although other AA transporters that recognize neutral AAs—including systems A, L, and ASC—also contribute. Of note, L-arginine was a less effective inhibitor than L-lysine and L-histidine, blocking only 41% of ^{18}F-AFETP uptake. This result suggests that ^{18}F-AFETP is not an ideal surrogate for arginine transport and may be due to different selectivities for the 4 families of AA transporters (y^+, y^+L, $b^{0,+}$AT, and $ATB^{0,+}$) that mediate most cationic AA transport. These properties may complicate the use of this tracer as a specific probe for cationic transport in vivo, and AAs with more basic side chains or other structural modifications may improve selectivity for cationic AA transporters.

The biodistribution studies with ^{18}F-AFETP in mice (Table 1) demonstrate good tumor uptake of radioactivity at 5, 30, and 60 min after injection, with higher uptake in tumor than in most normal tissues including the brain. Tumor-to-brain ratios ranged from 11:1 to 17:1, and the tumor–to–normal-tissue ratios at 30 and 60 min after injection were greater than 2:1 for the blood, bone fat, liver, muscle, and large intestine. These results are similar to prior studies using the 9 L gliosarcoma model, which demonstrated tumor-to-brain ratios of

approximately 15:1 at 30 and 60 min after injection (22). These results indicate that ^{18}F-AFETP tumor uptake is not cell-line-specific and may be useful for imaging tumors located in and outside the brain. The relatively low levels of activity in the bone indicate that no substantial in vivo defluorination occurred during the 60-min time course of the study. The highest levels of uptake at all time points in the study were observed in the kidneys and pancreas, a pattern frequently seen with radiolabeled AAs and similar to the biodistribution observed in the rat 9 L gliosarcoma model (22). The relatively high levels of ^{18}F-AFETP in the lungs and spleen are similar to the rat biodistribution pattern but are not observed with other ^{18}F-labeled AA targeting system L and system A transport systems (21,36,37). These differences in pulmonary and splenic uptake of activity may be related to the mechanism of transport of ^{18}F-AFETP, specifically the uptake via cationic AA transporters observed in vitro.

The results of small-animal PET demonstrate distinct patterns of tumor and normal brain uptake with each of the tracers evaluated. Significant differences among the uptake of ^{18}F-AFETP, ^{18}F-FDG, and ^{18}F-FET were observed in tumors and normal brain (Figs. 4 and 5). Of the 3 tracers evaluated, ^{18}F-AFETP provided the best brain tumor visualization, although this finding was primarily due to low uptake in normal brain, as discussed in detail below. All 3 tracers demonstrated relatively high uptake in the DBTs at both early (7.5–12.5 min) and late time points (47.5–57.5 min), with ^{18}F-FDG significantly greater than ^{18}F-FET greater than ^{18}F-AFETP. These tracers also differed substantially in their amount of uptake in normal brain, with ^{18}F-FDG significantly greater than ^{18}F-FET greater than ^{18}F-AFETP. These data are shown in Figure 6. Tumor visualization was achieved with all 3 tracers, although the uptake of ^{18}F-FDG in brain tumor was only slightly above that in normal brain at the conclusion of the 60-min study. As shown in Figure 7, the tumor-to-brain ratio at the late time points achieved with ^{18}F-AFETP was significantly higher than with ^{18}F-FDG and ^{18}F-FET ($P < 0.001$ for both). There was a trend toward higher tumor-to-brain ratios with ^{18}F-FET than with ^{18}F-FDG, but this did not reach statistical significance; this result may be due, in part, to less normal brain ^{18}F-FDG uptake because of the isoflurane anesthesia. The tumor-to-brain ratios observed with ^{18}F-AFETP in the small-animal PET studies were somewhat lower than those observed in the biodistribution studies, which may be due to partial-volume averaging in the brain tumors. Also, the tumor-to-brain ratios were constant in the small-animal PET studies using ^{18}F-AFETP but decreased at the 60-min time point in the biodistribution study. The reason for this difference is unclear but could be due to anesthesia effects on intracranial blood flow or AA transporter activity because the small-animal PET studies were conducted under anesthesia throughout the imaging period whereas the animals were anesthetized only during tracer injection for the biodistribution studies.

The relatively low normal brain uptake of ^{18}F-AFETP in the mouse DBT model warrants further consideration, because it provides both potential advantages and potential disadvantages for this tracer. The low brain uptake is a major factor in the higher tumor-to-brain ratios observed with ^{18}F-AFETP than with ^{18}F-FET and ^{18}F-FDG. Higher tumor–to–normal-tissue ratios can provide better tumor visualization and a larger dynamic range for assessing response to therapy. However, most low-grade tumors do not have grossly disrupted BBBs, and many high-grade gliomas, including glioblastoma, have nonenhancing regions not readily assessed with conventional contrast-enhanced MR imaging. One of the primary strengths of system L substrates such as ^{18}F-FET is their ability to cross the BBB and image the nonenhancing regions of gliomas more effectively than conventional MR imaging or ^{18}F-FDG (3,6,8,36). The low brain uptake of ^{18}F-AFETP is somewhat unexpected, because cationic AAs can cross the BBB via the CAT-1 transporter (38), and^{14}C-labeled L-histidinedemonstrated uptakesimilar to^{14}C-labeled methionine, tyrosine, and 3,4-dihydroxyphenylalanine in rat brain after intraarterial injection into the carotid artery (39). The reason for the low brain uptake in our studies is unclear, but possible

mechanisms include competition from endogenous AAs, lack of transport by CAT-1, and efflux transporters that mediate the clearance of ^{18}F-AFETP from the brain.

CONCLUSION

The nonnatural AA ^{18}F-AFETP has good tumor imaging properties in the mouse DBT model of glioblastoma, with rapid and persistent tumor uptake. High tumor-to-brain, tumor-to-muscle, and tumor-to-blood ratios were observed at 30 and 60 min after injection, with higher tumor-to-brain ratios than obtained with ^{18}F-FET or ^{18}F-FDG. In vitro assays demonstrate that the uptake of this tracer is mediated, in part, by cationic AA transporters. The relatively low brain uptake may limit visualization of nonenhancing gliomas, and ongoing work is aimed at developing analogs with greater brain availability and higher selectivity for cationic AA transport.

Acknowledgments

We thank Christopher Bognar and Shihong Li for synthesis and quality control of ^{18}F-FET and the Washington University Cyclotron Facility for ^{18}F-FDG and ^{18}F-fluoride production. We thank the Alvin J. Siteman Cancer Center at Washington University School of Medicine and Barnes-Jewish Hospital in St. Louis, Missouri, for the use of the Small Animal Cancer Imaging Core, which provided biodistribution and small-animal PET services.

References

1. Kaschten B, Stevenaert A, Sadzot B, et al. Preoperative evaluation of 54 gliomas by PET with fluorine-18-fluorodeoxyglucose and/or carbon-11-methionine. J Nucl Med. 1998; 39:778–785. [PubMed: 9591574]
2. Cook GJR, Maisey MN, Fogelman I. Normal variants, artefacts and interpretative pitfalls in PET imaging with 18-fluoro-2-deoxyglucose and carbon-11 methionine. Eur J Nucl Med. 1999; 26:1363–1378. [PubMed: 10541839]
3. Lau EWF, Drummond KJ, Ware RE, et al. Comparative PET study using F-18 FET and F-18 FDG for the evaluation of patients with suspected brain tumour. J Clin Neurosci. 2010; 17:43–49. [PubMed: 20004582]
4. Ogawa T, Inugami A, Hatazawa J, et al. Clinical positron emission tomography for brain tumors: comparison of [^{18}F]-fluorodeoxyglucose and L-methyl-^{11}C-methionine. AJNR. 1996; 17:345–353. [PubMed: 8938309]
5. Weber WA, Wester H-J, Grosu AL, et al. *O*-(2-[^{18}F]fluoroethyl)-L-tyrosine and L-[methyl-^{11}C]methionine uptake in brain tumours: initial results of a comparative study. Eur J Nucl Med. 2000; 27:542–549. [PubMed: 10853810]
6. Floeth FW, Pauleit D, Wittsack H-J, et al. Multimodal metabolic imaging of cerebral gliomas: positron emission tomography with [^{18}F]fluoroethyl-l-tyrosine and magnetic resonance spectroscopy. J Neurosurg. 2005; 102:318–327. [PubMed: 15739561]
7. Pauleit D, Floeth F, Hamacher K, et al. *O*-(2-[^{18}F]fluoroethyl)-l-tyrosine PET combined with MR imaging improves the diagnostic assessment of cerebral gliomas. Brain. 2005; 128:678–687. [PubMed: 15689365]
8. Pöpperl G, Götz C, Rachinger W, Gildehaus F-J, Tonn J-C, Tatsch K. Value of *O*-(2-[^{18}F]fluoroethyl)-L-tyrosine PET for the diagnosis of recurrent glioma. Eur J Nucl Med Mol Imaging. 2004; 31:1464–1470. [PubMed: 15248032]
9. Pöpperl G, Kreth FW, Herms J, et al. Analysis of ^{18}F-FET PET for grading of recurrent gliomas: is evaluation of uptake kinetics superior to standard methods? J Nucl Med. 2006; 47:393–403. [PubMed: 16513607]
10. Weckesser M, Langen KJ, Rickert CH, et al. *O*-(2-[^{18}F]fluorethyl)-L-tyrosine PET in the clinical evaluation of primary brain tumours. Eur J Nucl Med Mol Imaging. 2005; 32:422–429. [PubMed: 15650870]
11. Lieberman BP, Ploessl K, Wang L, et al. PET imaging of glutaminolysis in tumors by ^{18}F-(2*S*, 4*R*)-4-fluoroglutamine. J Nucl Med. 2011; 52:1947–1955. [PubMed: 22095958]

12. Laverman P, Boerman OC, Corstens FH, Oyen WJ. Fluorinated amino acids for tumour imaging with positron emission tomography. Eur J Nucl Med Mol Imaging. 2002; 29:681–690. [PubMed: 11976809]
13. Sutinen E, Jyrkkiö S, Alanen K, Någren K, Minn H. Uptake of [*N*-methyl-^{11}C]α-methylaminoisobutyric acid in untreated head and neck cancer studied by PET. Eur J Nucl Med Mol Imaging. 2003; 30:72–77. [PubMed: 12483412]
14. Uchino H, Kanai Y, Kim DK, et al. Transport of amino acid-related compounds mediated by L-type amino acid transporter 1 (LAT1): insights into the mechanisms of substrate recognition. Mol Pharmacol. 2002; 61:729–737. [PubMed: 11901210]
15. Fuchs BC, Bode BP. Amino acid transporters ASCT2 and LAT1 in cancer: partners in crime? Semin Cancer Biol. 2005; 15:254–266. [PubMed: 15916903]
16. Nawashiro H, Otani N, Shinomiya N, et al. L-type amino acid transporter 1 as a potential molecular target in human astrocytic tumors. Int J Cancer. 2006; 119:484–492. [PubMed: 16496379]
17. Qu W, Oya S, Lieberman BP, et al. Preparation and characterization of L-[5-^{11}C]-glutamine for metabolic imaging of tumors. J Nucl Med. 2012; 53:98–105. [PubMed: 22173839]
18. Qu W, Zha Z, Ploessl K, et al. Synthesis of optically pure 4-fluoroglutamines as potential metabolic imaging agents for tumors. J Am Chem Soc. 2011; 133:1122–1133. [PubMed: 21190335]
19. Qu W, Zha Z, Lieberman BP, et al. Facile synthesis [5-(13)C-4-(2)H(2)]-L-glutamine for hyperpolarized MRS imaging of cancer cell metabolism. Acad Radiol. 2011; 18:932–939. [PubMed: 21658976]
20. Krasikova RN, Kuznetsova OF, Fedorova OS, et al. 4-[^{18}F]fluoroglutamic acid (BAY 85-8050), a new amino acid radiotracer for PET imaging of tumors: synthesis and in vitro characterization. J Med Chem. 2011; 54:406–410. [PubMed: 21128591]
21. McConathy J, Martarello L, Malveaux EJ, et al. Radiolabeled amino acids for tumor imaging with PET:radiosynthesis and biological evaluation of 2-Amino-3-[^{18}F]fluoro-2-methylpropanoic acid and 3-[^{18}F]fluoro-2-methyl-2-(methylamino) propanoic acid. J Med Chem. 2002; 45:2240–2249. [PubMed: 12014962]
22. McConathy J, Zhou D, Shockley SE, et al. Click synthesis and biologic evaluation of *(R)*- and *(S)*-2-amino-3-[1-(2-[^{18}F]fluoroethyl)-^{1}H-[1,2,3]triazol-4-yl] propanoic acid for brain tumor imaging with positron emission tomography. Mol Imaging. 2010; 9:329–342. [PubMed: 21084029]
23. McConathy J, Martarello L, Malveaux EJ, et al. Synthesis and evaluation of 2-amino-4-[^{18}F]fluoro-2-methylbutanoic acid (FAMB): relationship of amino acid transport to tumor imaging properties of branched fluorinated amino acids. Nucl Med Biol. 2003; 30:477–490. [PubMed: 12831985]
24. Yu W, McConathy J, Olson J, Camp VM, Goodman MM. Facile stereospecific synthesis and biological evaluation of (*S*)- and (*R*)-2-amino-2-methyl-4-[^{123}I] iodo-3-(*E*)-butenoic acid for brain tumor imaging with single photon emission computerized tomography. J Med Chem. 2007; 50:6718–6721. [PubMed: 18052089]
25. Gupta N, Prasad PD, Ghamande S, et al. Up-regulation of the amino acid transporter ATB(0,+) (SLC6A14) in carcinoma of the cervix. Gynecol Oncol. 2006; 100:8–13. [PubMed: 16168467]
26. Gupta N, Miyauchi S, Martindale RG, et al. Upregulation of the amino acid transporter ATB$^{0,+}$ (SLC6A14) in colorectal cancer and metastasis in humans. Biochim Biophys Acta. 2005; 1741:215–223. [PubMed: 15905073]
27. O'Kane RL, Vina JR, Simpson I, Zaragoza R, Mokashi A, Hawkins RA. Cationic amino acid transport across the blood-brain barrier is mediated exclusively by system y+ Am J Physiol Endocrinol Metab. 2006; 291:E412–E419. [PubMed: 16569760]
28. Dillon BJ, Prieto VG, Curley SA, et al. Incidence and distribution of arginino-succinate synthetase deficiency in human cancers. Cancer. 2004; 100:826–833. [PubMed: 14770441]
29. Yang TS, Lu SN, Chao Y, et al. A randomised phase II study of pegylated arginine deiminase (ADI-PEG 20) in Asian advanced hepatocellular carcinoma patients. Br J Cancer. Aug 31.2010

30. Jost SC, Wanebo JE, Song S-K, et al. In vivo imaging in a murine model of glioblastoma. Neurosurgery. 2007; 60:360–370. [PubMed: 17290188]

31. Tang G, Tang X, Wang M, Luo L, Gan M, Huang Z. Automated commercial synthesis system for preparation of *O*-(2-[^{18}F]fluoroethyl)-L-tyrosine by direct nucleophilic displacement on a resin column. J Labelled Comp Radiopharm. 2003; 46:661–668.

32. Zuhayra M, Alfteimi A, Forstner CV, Lützen U, Meller B, Henze E. New approach for the synthesis of [^{18}F]fluoroethyltyrosine for cancer imaging: simple, fast, and high yielding automated synthesis. Bioorg Med Chem. 2009; 17:7441–7448. [PubMed: 19804977]

33. Gazzola GC, Dall'Asta V, Franchi-Gazzola R, White MF. The cluster-tray method for rapid measurement of solute fluxes in adherent cultured cells. Anal Biochem. 1981; 115:368–374. [PubMed: 7304965]

34. Mourad PD, Farrell L, Stamps LD, Chicoine MR, Silbergeld DL. Why are systemic glioblastoma metastases rare? Systemic and cerebral growth of mouse glioblastoma. Surg Neurol. 2005; 63:511–519. [PubMed: 15936366]

35. Jost SC, Collins L, Travers S, Piwnica-Worms D, Garbow JR. Measuring brain tumor growth: combined bioluminescence imaging-magnetic resonance imaging strategy. Mol Imaging. 2009; 8:245–253. [PubMed: 19796602]

36. Langen K-J, Hamacher K, Weckesser M, et al. *O*-(2-[^{18}F]fluoroethyl)-L-tyrosine: uptake mechanisms and clinical applications. Nucl Med Biol. 2006; 33:287–294. [PubMed: 16631076]

37. Tsukada H, Sato K, Fukumoto D, Nishiyama S, Harada N, Kakiuchi T. Evaluation of d-isomers of *O*-^{11}C-methyl tyrosine and *O*-^{18}F-fluoromethyl tyrosine as tumor-imaging agents in tumor-bearing mice: comparison with l- and d-^{11}C-methionine. J Nucl Med. 2006; 47:679–688. [PubMed: 16595503]

38. Hatzoglou M, Fernandez J, Yaman I, Closs E. Regulation of cationic amino acid transport: the story of the CAT-1 transporter. Annu Rev Nutr. 2004; 24:377–399. [PubMed: 15459982]

39. Oldendorf WH. Brain uptake of radiolabeled amino acids, amines, and hexoses after arterial injection. Am J Physiol. 1971; 221:1629–1639. [PubMed: 5124307]

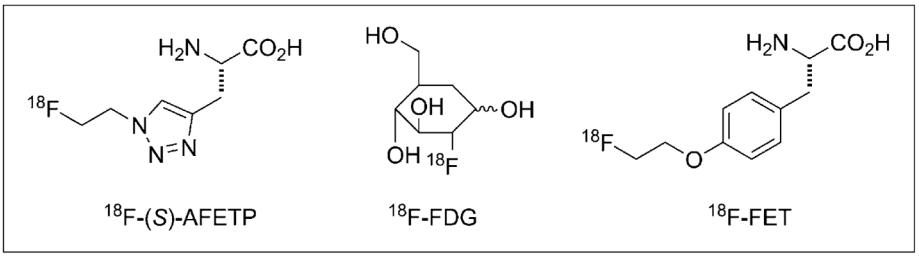

FIGURE 1.
Structures of ^{18}F-labeled PET tracers evaluated in the mouse DBT glioma model.

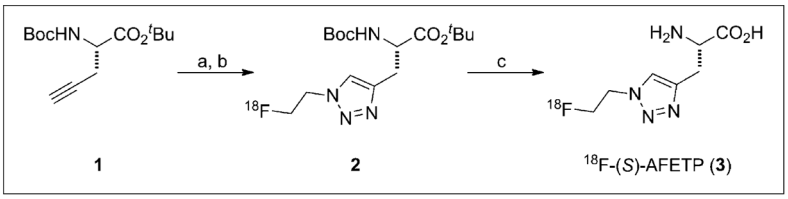

FIGURE 2.

Radiosynthesis of ^{18}F-AFETP. (A) $CuSO_4$, sodium ascorbate, *N,N*-dimethylformamide/water 2-^{18}F-fluoroethyl azide. (B) HPLC purification. (C) 1 M aqueous HCl, 60W microwave.

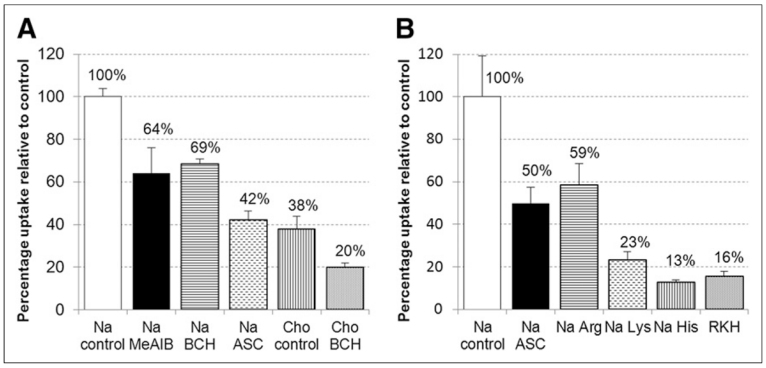

FIGURE 3.

In vitro uptake of ^{18}F-AFETP by DBT glioma cells in presence of neutral (A) and cationic (B) competitive inhibitors of the amino acid transport. Uptake data are normalized based on amount of activity added to each well and total amount of protein in each well. Data are expressed as percentage uptake relative to sodium control condition, and values for each condition are noted in appropriate bars. To provide consistent osmolarity, compared with inhibitory conditions, Na control and Cho controls contain 10 mM sucrose. ASC = 3.3 mM each of L-Ala, L-Ser, L-Cys; BCH = 10 mM 2-aminobicyclo(2,2,1)-heptane-2-carboxylic acid (system L inhibitor); Cho = assay buffer containing choline ions; MeAIB = 10 mM *N*-methyl, α-aminoisobutryic acid (system A inhibitor); Na = assay buffer containing sodium ions; RKH = 3.3 mM each of L-arginine, L-lysine, and L-histidine.

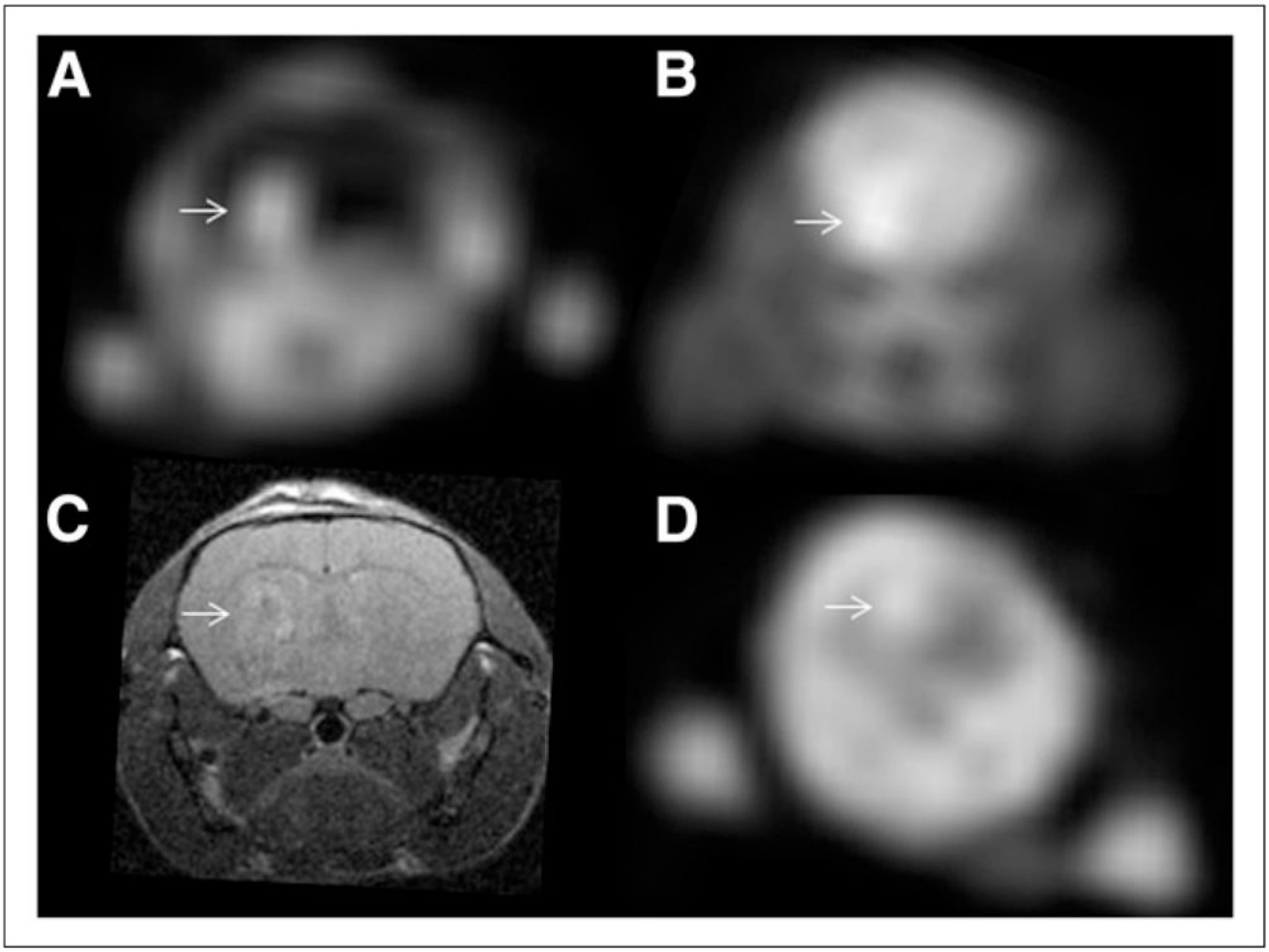

FIGURE 4.

Representative small-animal PET and MR images from mice with intracranial DBTs. Small-animal PET images in A and B and MR image in C were obtained from same animal, whereas small-animal PET image in D was from mouse in different cohort. Tumors are indicated in each panel with arrows. (A, B, and D) Summed images from 50 to 60 min after injection of ^{18}F-AFETP (A), ^{18}F-FDG (B), or ^{18}F-FET (D). MR image (C) was obtained usingT2-weighted sequence, as described in "Materials and Methods" section. Tumors were confirmed histologically (data not shown).

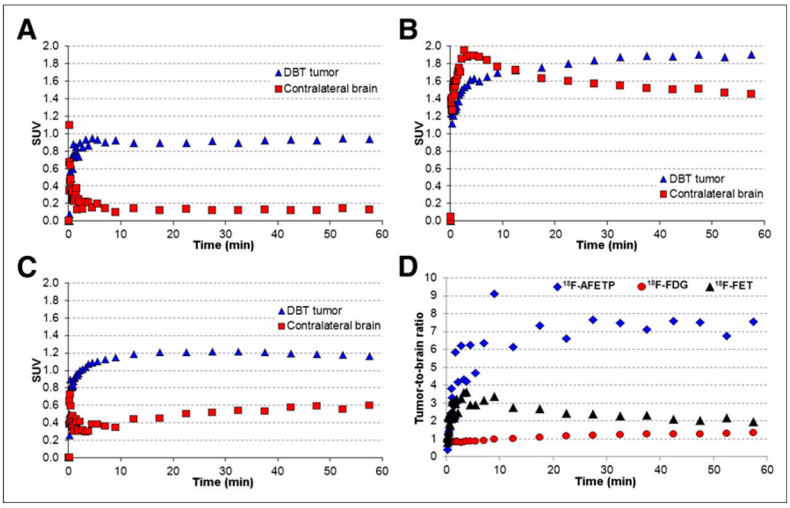

FIGURE 5.

Representative time–activity curves and tumor-to-brain ratio curves observed with dynamic small-animal PET studies in mice with intracranial DBTs. Time–activity curves for ^{18}F-AFETP (A), ^{18}F-FDG (B), and ^{18}F-FET (C) are displayed as average SUVs. ^{18}F-AFETP and ^{18}F-FDG data in A and B were obtained in same animal, whereas ^{18}F-FET data in C was from animal from different cohort. Data from time–activity curves are expressed as tumor-to-brain ratios over time for all 3 tracers in D. Figure 6 shows average data from these small-animal PET studies from all animals (n = 3 or 4) for each tracer.

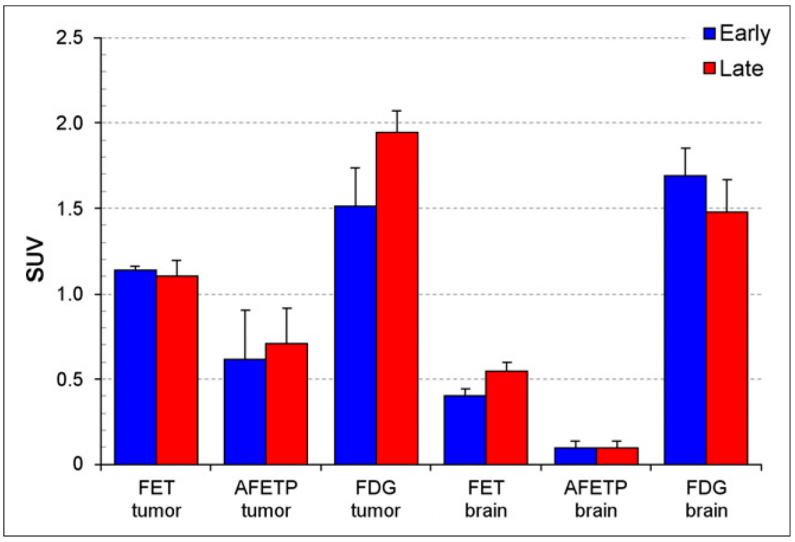

FIGURE 6.

Average SUVs in intracranial DBTs and contralateral normal brain measured through small-animal PET studies performed with ^{18}F-FET (n = 3), ^{18}F-AFETP (n = 4), and ^{18}F-FDG (n = 4). Early (7–12.5 min) and late (47.5–57.5 min) time points are depicted. Small-animal PET data for ^{18}F-AFETP and ^{18}F-FDG were obtained in same animals, whereas ^{18}F-FET data were obtained in second cohort of animals. Error bars show SD.

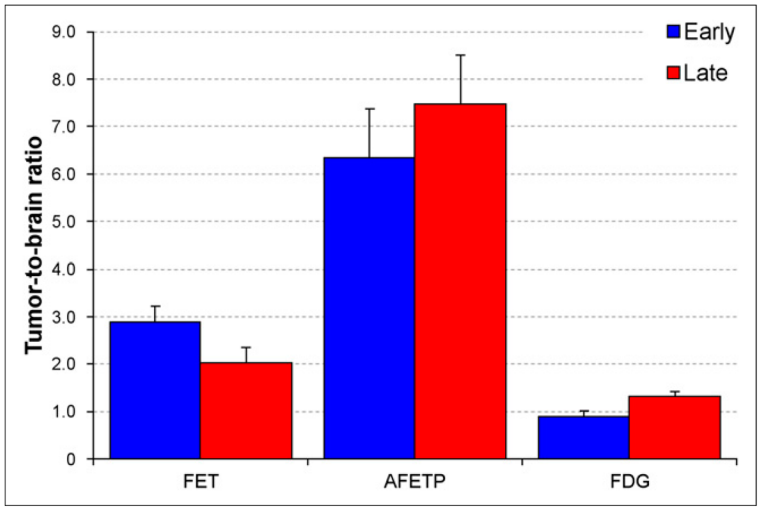

FIGURE 7.

Tumor-to-brain ratios between intracranial DBTs and contralateral normal brain measured through small-animal PET studies performed with ^{18}F-FET (n = 3), ^{18}F-AFETP (n = 4), and ^{18}F-FDG (n = 4). Data for early (7–12.5 min) and late (47.5–57.5 min) time points are depicted. Small-animal PET data for ^{18}F-AFETP and ^{18}F-FDG were obtained in same animals, whereas ^{18}F-FET data were obtained in second cohort of animals. Error bars show SD.

TABLE 1

Biodistribution of ^{18}F-AFETP in BALB/c Mice with Intracranial DBTs

Organ or tissue	5 min	30 min	60 min
Blood	3.99 ± 0.38	1.66 ± 0.20	0.69 ± 0.18
Bone	0.91 ± 0.17	1.46 ± 0.14	0.99 ± 0.47
Brain	0.25 ± 0.03	0.34 ± 0.40	0.23 ± 0.03
Fat	0.90 ± 0.08	0.61 ± 0.20	0.39 ± 0.17
Heart	2.19 ± 0.19	2.10 ± 0.33	1.64 ± 0.27
Kidney	65.6 ± 10.2	51.4 ± 6.2	17.8 ± 3.7
Large intestine	1.81 ± 0.39	1.79 ± 0.24	1.08 ± 0.29
Liver	3.19 ± 0.50	1.56 ± 0.15	0.65 ± 0.12
Lung	6.06 ± 0.95	5.53 ± 1.87	2.40 ± 0.67
Muscle	1.34 ± 0.19	1.22 ± 0.12	1.02 ± 0.12
Pancreas	36.1 ± 5.1	21.9 ± 4.1	8.75 ± 3.0
Salivary glands	5.23 ± 0.41	2.96 ± 0.46	1.28 ± 0.22
Small intestine	3.97 ± 0.90	2.56 ± 0.38	1.42 ± 0.27
Spleen	3.40 ± 0.42	2.67 ± 0.20	1.67 ± 0.27
Tumor	4.39 ± 1.10	4.91 ± 1.15	2.46 ± 1.02

Data are expressed as %ID/g ± SD; n = 3 or 4 for each value.